NASA TN D-1931

29 p.



# TECHNICAL NOTE

D-1931

## STATIC STABILITY CHARACTERISTICS OF MODELS OF THE BLUE SCOUT AND THE BLUE SCOUT, JR., RESEARCH VEHICLES AT MACH NUMBERS FROM 2.29 TO 3.75

By Lloyd S. Jernell

Langley Research Center
Langley Station, Hampton, Va.

NATIONAL AERONAUTICS AND SPACE ADMINISTRATION
WASHINGTON
July 1963

NATIONAL AERONAUTICS AND SPACE ADMINISTRATION

TECHNICAL NOTE D-1931

# STATIC STABILITY CHARACTERISTICS OF MODELS OF THE BLUE SCOUT AND THE BLUE SCOUT, JR., RESEARCH VEHICLES AT MACH NUMBERS FROM 2.29 TO 3.75

By Lloyd S. Jernell

## SUMMARY



An investigation has been conducted at Mach numbers from 2.29 to 3.75 to determine the static longitudinal and lateral stability characteristics of a 0.067-scale model of the Blue Scout research vehicle and a 0.10-scale model of the Blue Scout, Jr.

The results indicated a slight forward shift in center of pressure with increasing Mach number for both complete models. A small amount of flare-fin interference effect was exhibited by the Blue Scout configuration. Also, an interference between the forward and rearward fins was evident on the Blue Scout, Jr., configurations. Both models indicated a relatively small positive effective dihedral near $\alpha = 0^{\circ}$; however, at $\alpha = 5^{\circ}$ the effective dihedral becomes highly negative, especially at the lower test Mach number.

## INTRODUCTION

Recent research has been directed toward development of a family of solid-fuel research vehicles designated as the Hyper-Environmental Test System (HETS) 609-A. These vehicles are capable of performing a variety of missions, including high-altitude probing and spacecraft orbiting. The vehicles are similar in many respects to the Scout vehicles of the National Aeronautics and Space Administration. The results of investigations of several Scout configurations are presented in references 1 to 4.

Models of two configurations, the Blue Scout and the Blue Scout, Jr., have been investigated at the NASA Langley Research Center. The investigations were made in the Langley Unitary Plan wind tunnel at Mach numbers from 2.29 to 3.75 to determine the effects of fins, first-stage flare, antennas, and wiring tunnels on the static longitudinal and lateral stability characteristics of a 0.067-scale model of the Blue Scout configuration and the effect of fins on the stability characteristics of a 0.10-scale model of the Blue Scout, Jr., configuration.

## SYMBOLS

The data presented are referenced to the body-axes system (fig. 1). The location of the moment center for each model is shown on the model drawings (fig. 2). Symbols used are defined as follows:

| | |
|---|---|
| $A$ | maximum cylindrical cross-section area, sq ft |
| $C_A$ | axial-force coefficient, $\frac{\text{Axial force}}{qA}$ |
| $C_{A,b}$ | base axial-force coefficient, $\frac{\text{Base axial force}}{qA}$ |
| $C_l$ | rolling-moment coefficient, $\frac{\text{Rolling moment}}{qAd}$ |
| $C_m$ | pitching-moment coefficient, $\frac{\text{Pitching moment}}{qAd}$ |
| $C_N$ | normal-force coefficient, $\frac{\text{Normal force}}{qA}$ |
| $C_n$ | yawing-moment coefficient, $\frac{\text{Yawing moment}}{qAd}$ |
| $C_Y$ | side-force coefficient, $\frac{\text{Side force}}{qA}$ |
| $d$ | maximum cylindrical diameter, in. |
| $l$ | length of model, in. |
| $M$ | free-stream Mach number |
| $q$ | free-stream dynamic pressure, lb/sq ft |
| $R$ | radius |
| $x,y,z$ | body axes |
| $x_{cp}$ | position of center of pressure measured from nose, in. |
| $\alpha$ | angle of attack referred to model center line, deg |
| $\beta$ | angle of sideslip, referred to model center line, deg |

Model component identification:

Blue Scout configuration:

| | |
|---|---|
| $A_1$ | antennas |
| $B_1$ | body |
| $F_1$ | fins |
| $S_1$ | first-stage flare |
| $T_1$ | wiring tunnels |

Blue Scout, Jr., configuration:

| | |
|---|---|
| $B_2$ | body |
| $F_{21}$ | forward fins |
| $F_{22}$ | aft fins |

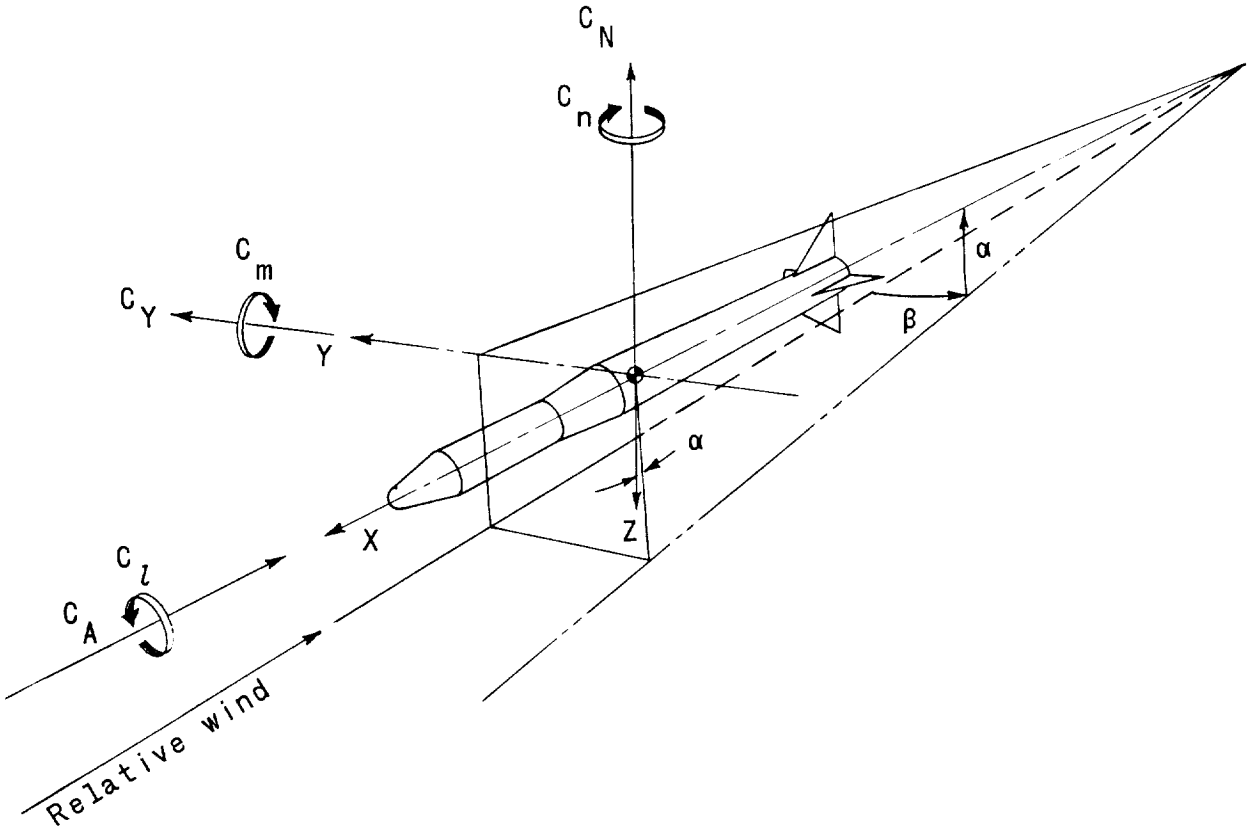


Figure 1.- System of axes. Arrows indicate positive direction.

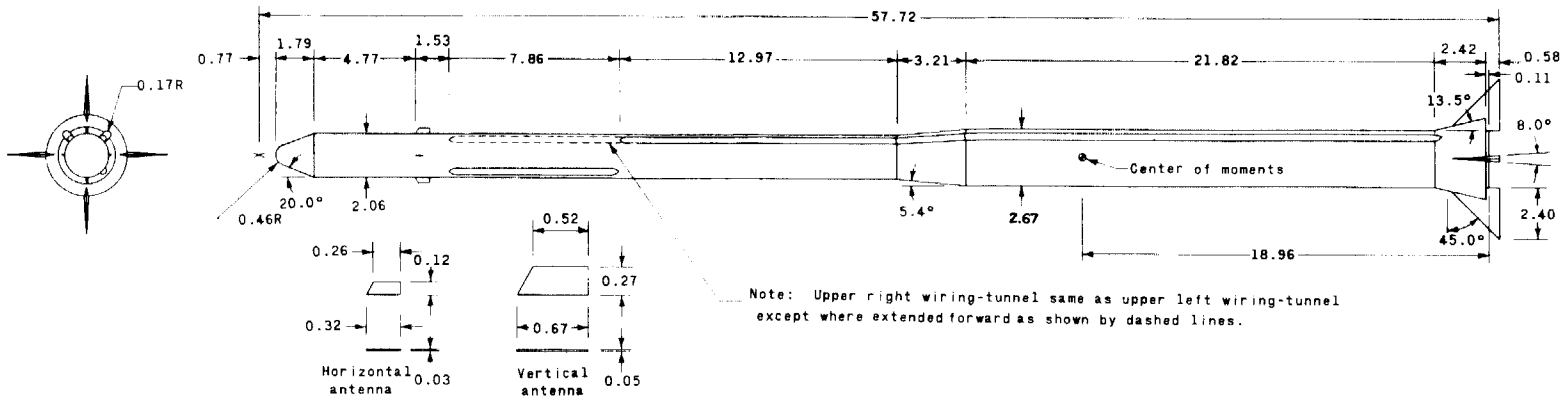


0.067-scale model of the Blue Scout configuration

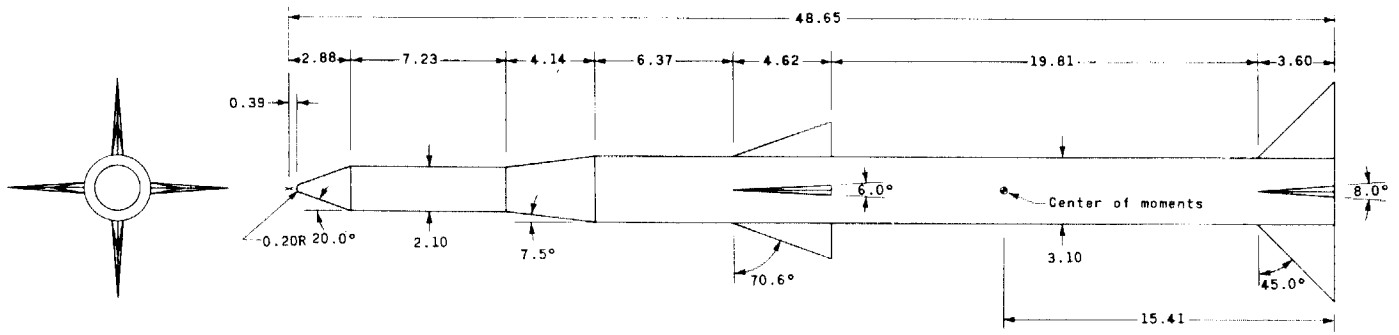


0.100-scale model of the Blue Scout, Jr., configuration

Figure 2.- Drawings of models of the Blue Scout and Blue Scout, Jr., configurations of the HETS 609-A test vehicle. (Dimensions are in inches unless otherwise indicated.)

## MODEL, APPARATUS, AND MEASUREMENTS

Drawings of the models are shown in figure 2. The Blue Scout model represents a four-stage configuration with a length-diameter ratio of about 22. The model components consist of four fins in a cruciform arrangement, a 13.5° first-stage flare, antennas, and wiring tunnels. The fins were of delta planform and had 8°-wedge airfoil sections.

The Blue Scout, Jr., model represents a four-stage configuration with a length-diameter ratio of about 16. Four delta planform fins were incorporated in a cruciform arrangement at the bases of the first and second stages. The rearward or first-stage fins had a leading-edge sweep angle of 45° and an 8°-wedge airfoil section. The forward (or second-stage) fins had a 70.6° leading-edge sweep angle and a 6°-wedge airfoil section.

The tests were conducted in the Langley Unitary Plan wind tunnel. This is a variable-pressure continuous-flow tunnel having a Mach number range from about 1.5 to 4.7. Each of the two test sections is 4 feet square by approximately 7 feet long and employs an asymmetric sliding-block nozzle, allowing a variation in Mach number without tunnel shutdown.

Aerodynamic forces and moments were measured by means of a sting-supported, internally mounted, six-component strain-gage balance. The base pressure was measured by means of static orifices located at the model base and within the balance cavity.

Schlieren photographs were obtained for each configuration. Flow patterns of one of the configurations (Model $B_1S_1$) at $M = 2.45$ are presented in figure 3.

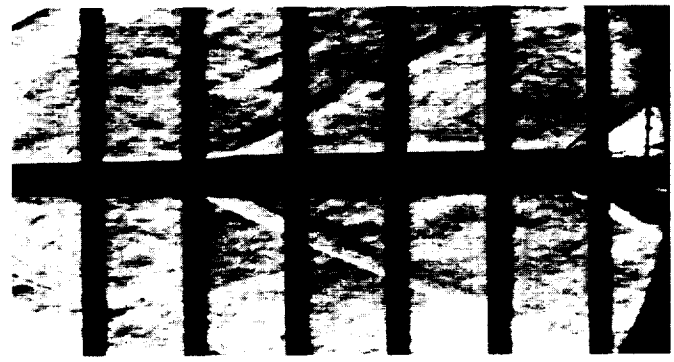

$\alpha = 0°$

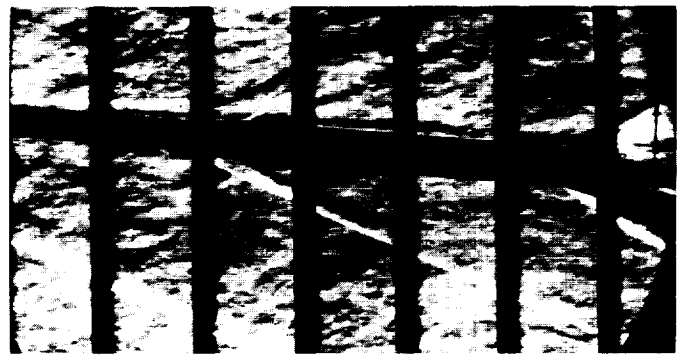

$\alpha = 6°$

L-63-3149

Figure 3.- Typical schlieren photographs of model $B_1S_1$, $M = 2.45$.

## TESTS

Tests were conducted on all configurations through an angle-of-attack range of approximately -6° to 6° at zero angle of sideslip. Data were obtained both on the bodies alone and in combination with the various components (fins, antenna, etc.). In addition, data were obtained on some configurations through an angle-of-sideslip range

of approximately -6° to 6° for angles of attack of 0° and 5°. The stagnation temperature was maintained at 150° F throughout the tests. The dewpoint was held below -30° F to prevent excessive moisture condensation.

The data of reference 3, which were obtained for a model similar in size and geometry to the Blue Scout model, indicate that for the Mach number and Reynolds number ranges of this investigation the effect of Reynolds number on the aerodynamic characteristics is negligible. Hence, in order to obtain the best possible data accuracy, the test dynamic pressure was limited only by the balance load capabilities and the available tunnel operating power, thereby varying the Reynolds number considerably throughout the investigation. The limits of this variation are as follows:

| M | Reynolds number per ft |
|---|---|
| 2.29 | 2.1 to 5.3 × $10^6$ |
| 2.45 | 4.0 |
| 2.87 | 4.6 |
| 2.96 | 2.4 to 7.0 |
| 3.75 | 2.7 to 7.0 |

## CORRECTIONS AND ACCURACIES

The angles of attack and sideslip have been corrected for wind-tunnel flow misalinement and model-support-system deflection under load.

The axial-force coefficients have been adjusted to a condition of free-stream static pressure at the base of the models. Typical increments used in this adjustment are shown in figures 4 and 5.

The estimated accuracies of the individual measured quantities are as follows:

| | |
|---|---|
| $C_A$ | ±0.010 |
| $C_l$ | ±0.002 |
| $C_m$ | ±0.015 |
| $C_N$ | ±0.020 |
| $C_n$ | ±0.015 |
| $C_Y$ | ±0.020 |
| $\alpha$, deg | ±0.10 |
| $\beta$, deg | ±0.10 |
| M | ±0.015 |

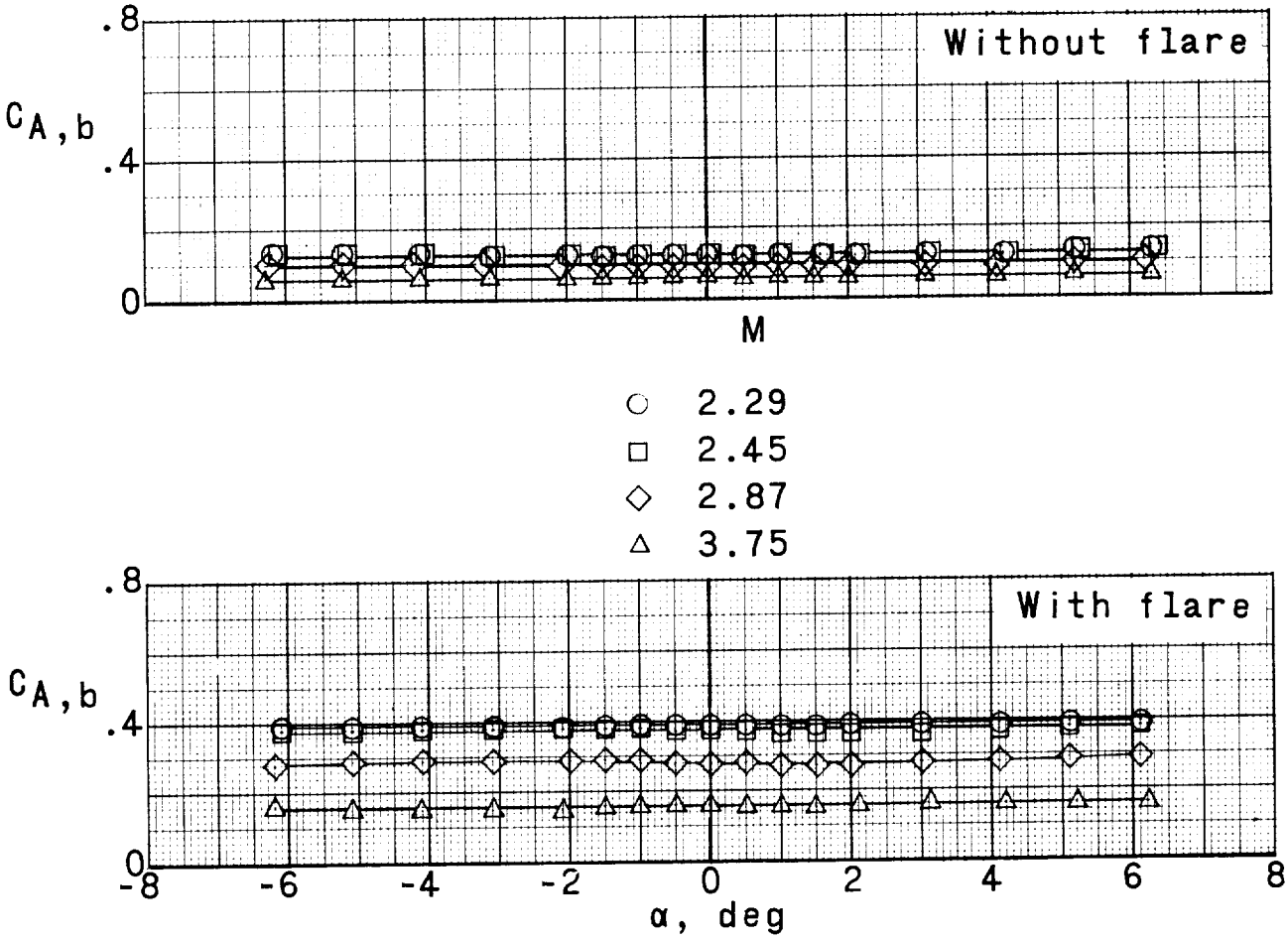


Figure 4.- Typical variation of base axial-force coefficient with angle of attack for a 0.067-scale model of the Blue Scout configuration with and without flare.

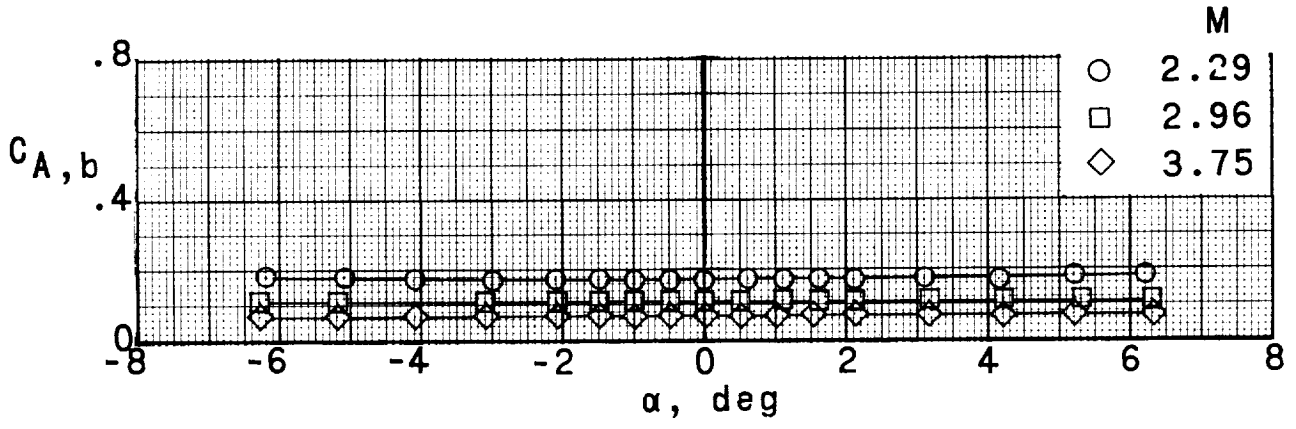


Figure 5.- Typical variation of base axial-force coefficient with angle of attack for a 0.100-scale model of the Blue Scout, Jr., configuration.

## RESULTS AND DISCUSSION

### Blue Scout Configuration

The aerodynamic characteristics in pitch for the Blue Scout model are presented in figure 6. The normal-force and pitching-moment characteristics of the body-alone configuration $B_1$ (fig. 6(a)) are relatively linear between $\alpha = \pm 4^\circ$ and essentially invariant with test Mach number. Results for model $B_1S_1$ show that the addition of the flare (fig. 6(b)) causes an increase in the slope of the normal-force curve and a corresponding increase in the model stability, with the stability increment decreasing as angle of attack is increased. Data for model $B_1F_1$ at the lower Mach numbers show that the addition of the fins (fig. 6(c)) results in a greater increase in normal force than that caused by the flare addition. However, there is a loss in fin normal force with Mach number and, at $M = 3.75$, the $C_{N_\alpha}$ for the finned and flared bodies are approximately equal. As expected, the decrease in fin normal force with increasing Mach number is accompanied by a corresponding decrease in the stability of the finned model. It is interesting to note that for the higher Mach numbers the flared body has greater stability near zero angle of attack than does the finned model. However, this condition exists for only a small angle-of-attack range ($\alpha \approx \pm 1^\circ$) because of the nonlinear variation of $C_m$ with $\alpha$ for the flared body.

The characteristics of the body-flare-fin configuration $B_1S_1F_1$ are shown in figure 6(d). The separate effects of the flare and fins on $C_m$ and $C_N$ is greater than the effect exhibited by the flare-fin combination and this result indicates the existence of a small amount of flare-fin interference. Data for $B_1S_1F_1T_1$ show that the addition of the wiring tunnels to the configuration (fig. 6(e)) has no noticeable effect on $C_N$ and, in the range $1^\circ \leqq \alpha \leqq 6^\circ$, little effect on $C_m$. However, for the range $-6^\circ \leqq \alpha \leqq 1^\circ$ there is some reduction in the model stability. For configuration $B_1S_1F_1T_1A_1$, the addition of the antennas (fig. 6(f)) apparently has little or no effect on the normal-force or pitching-moment coefficients.

Figure 7 presents the center-of-pressure location as a fraction of body length for angles of attack of $2^\circ$ and $4^\circ$ for the Blue Scout model. The data indicate that for the angles of attack presented there is little change in the center-of-pressure location with test Mach number for the complete configuration $(B_1S_1F_1T_1A_1)$. As expected, the fin-body configuration $B_1F_1$ exhibits a forward movement of the center of pressure with increasing Mach number, corresponding to the loss in fin normal force. It should be noted that all configurations which include the flare show a forward movement of the center of pressure as the angle of attack is increased from $2^\circ$ to $4^\circ$.

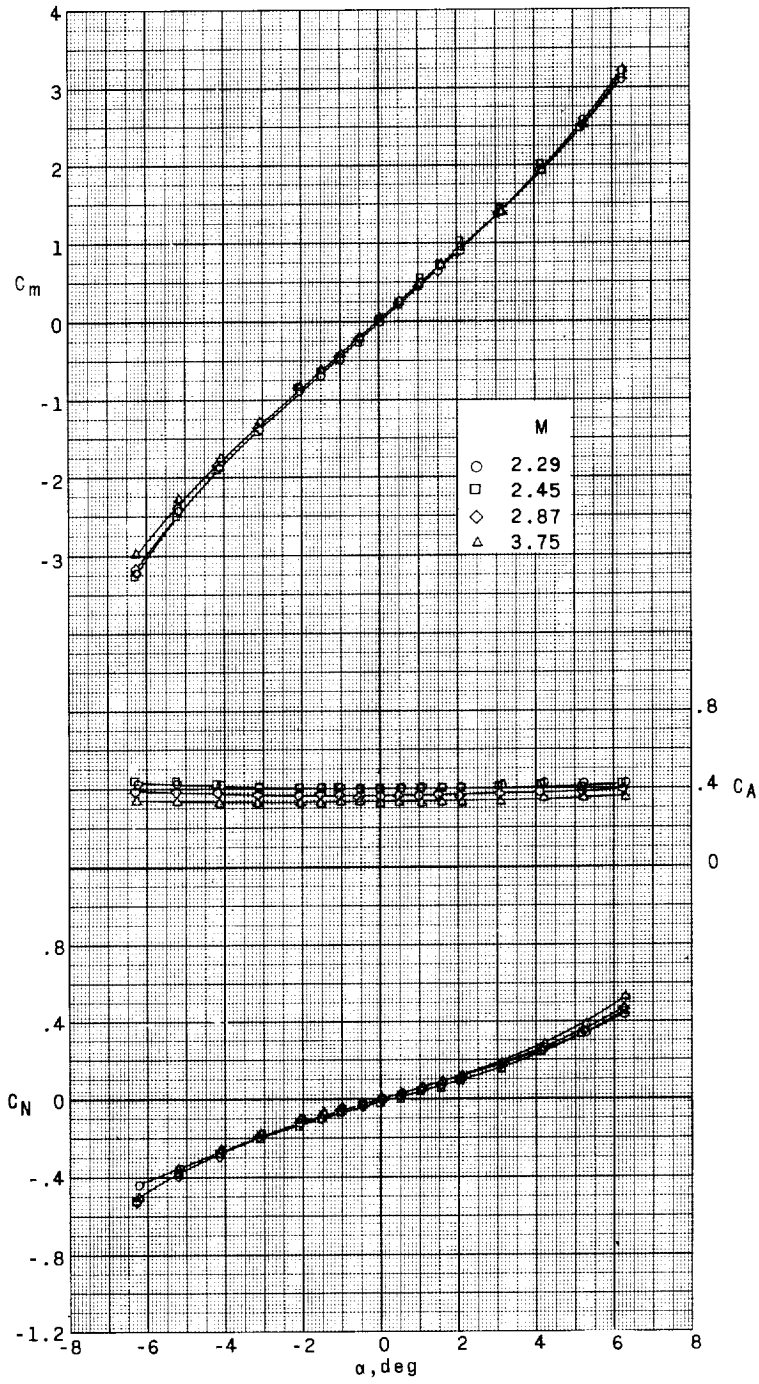


(a) Model $B_1$.

Figure 6.- Aerodynamic characteristics in pitch of a 0.067-scale model of the Blue Scout configuration.

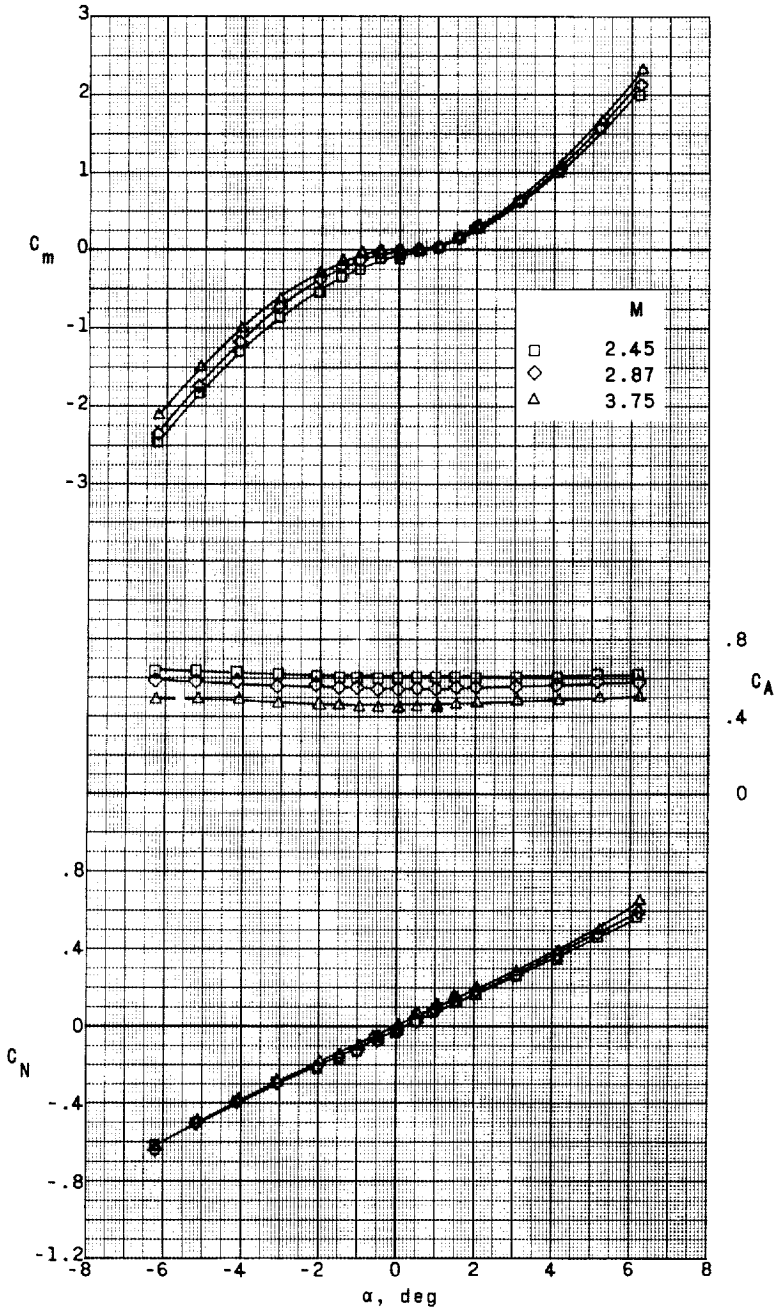


(b) Model $B_1S_1$.

Figure 6.- Continued.

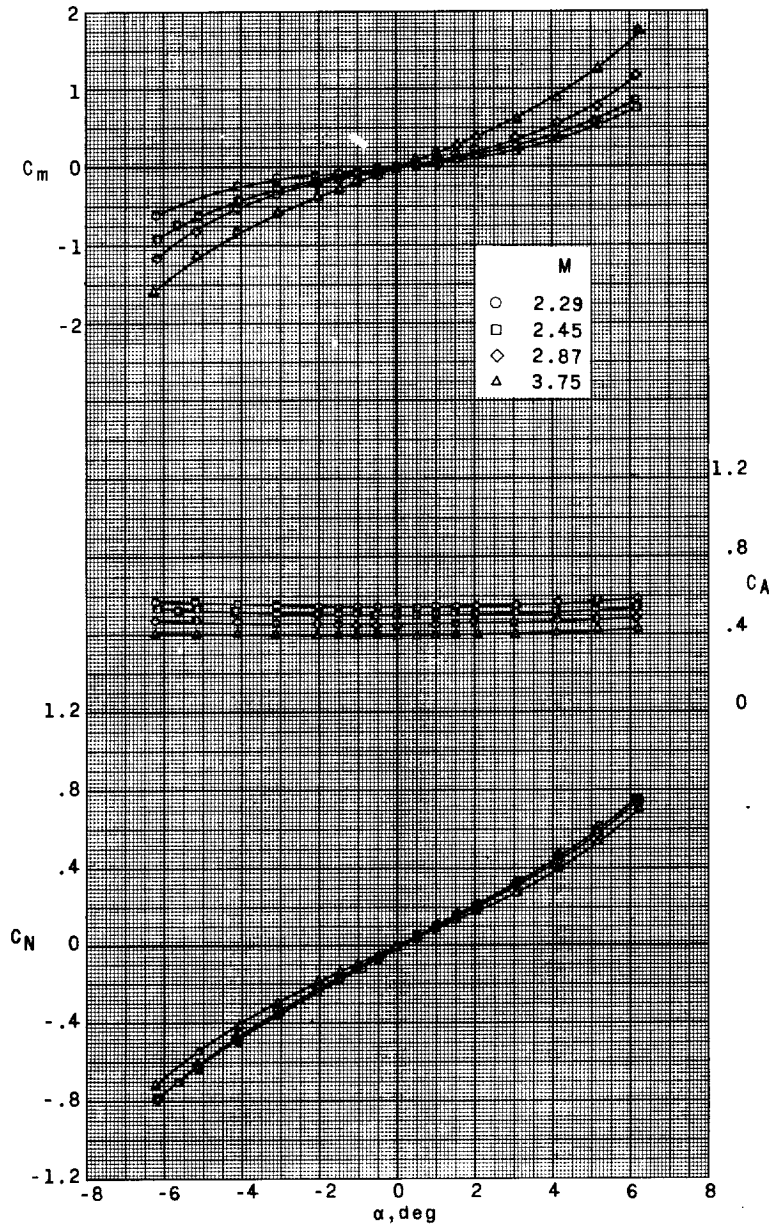


(c) Model $B_1F_1$.

Figure 6.- Continued.

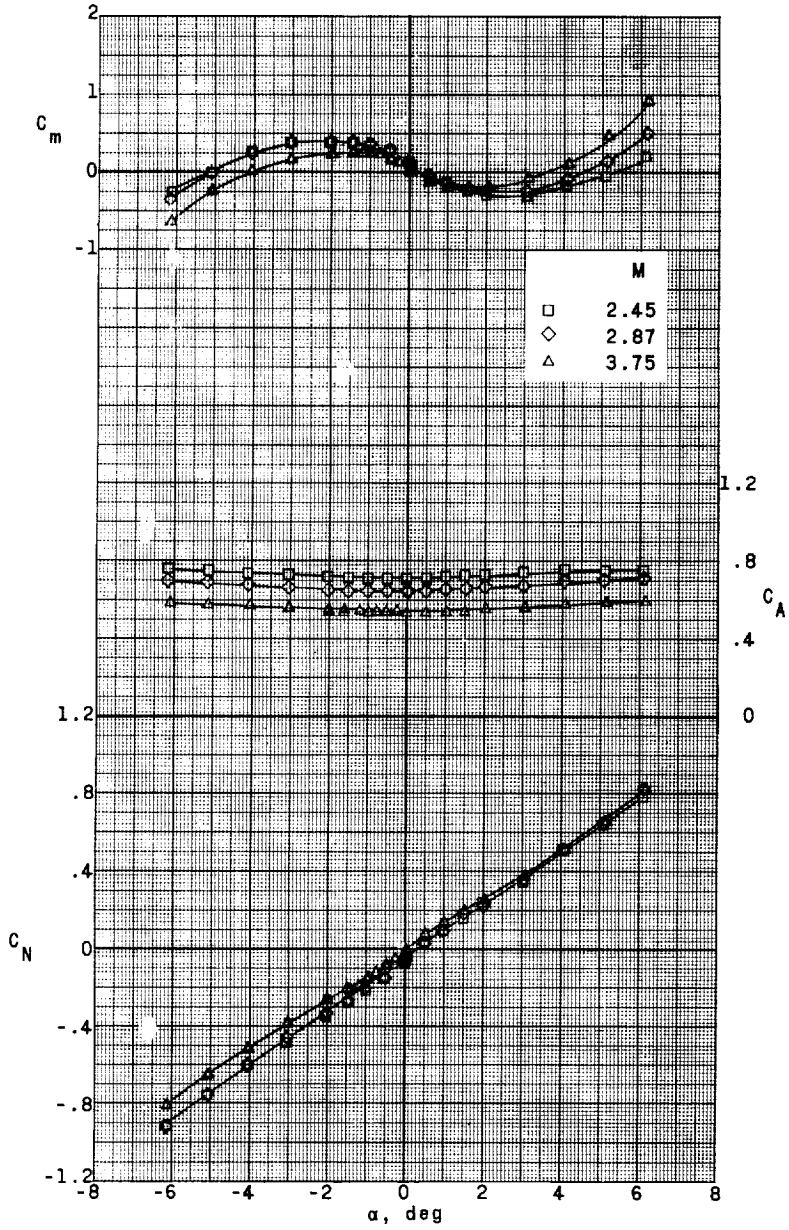


(d) Model $B_1S_1F_1$.

Figure 6.- Continued.

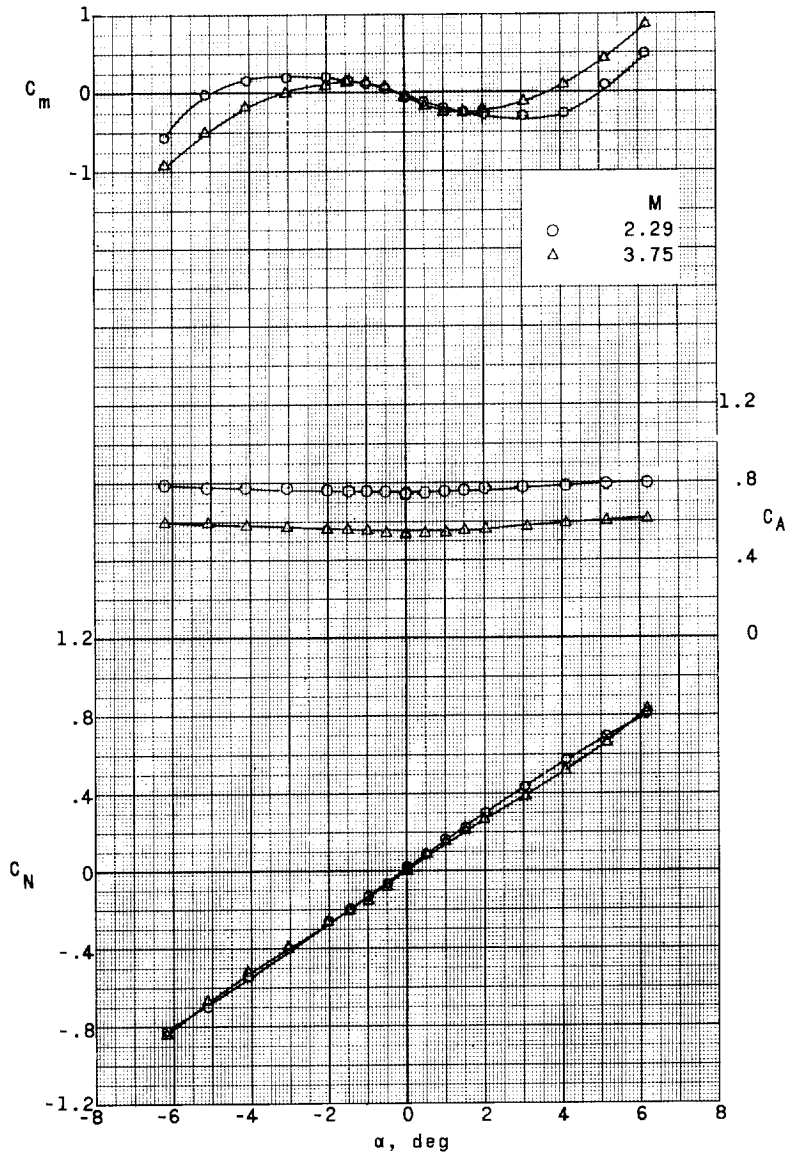


(e) Model $B_1S_1F_1T_1$.

Figure 6.- Continued.

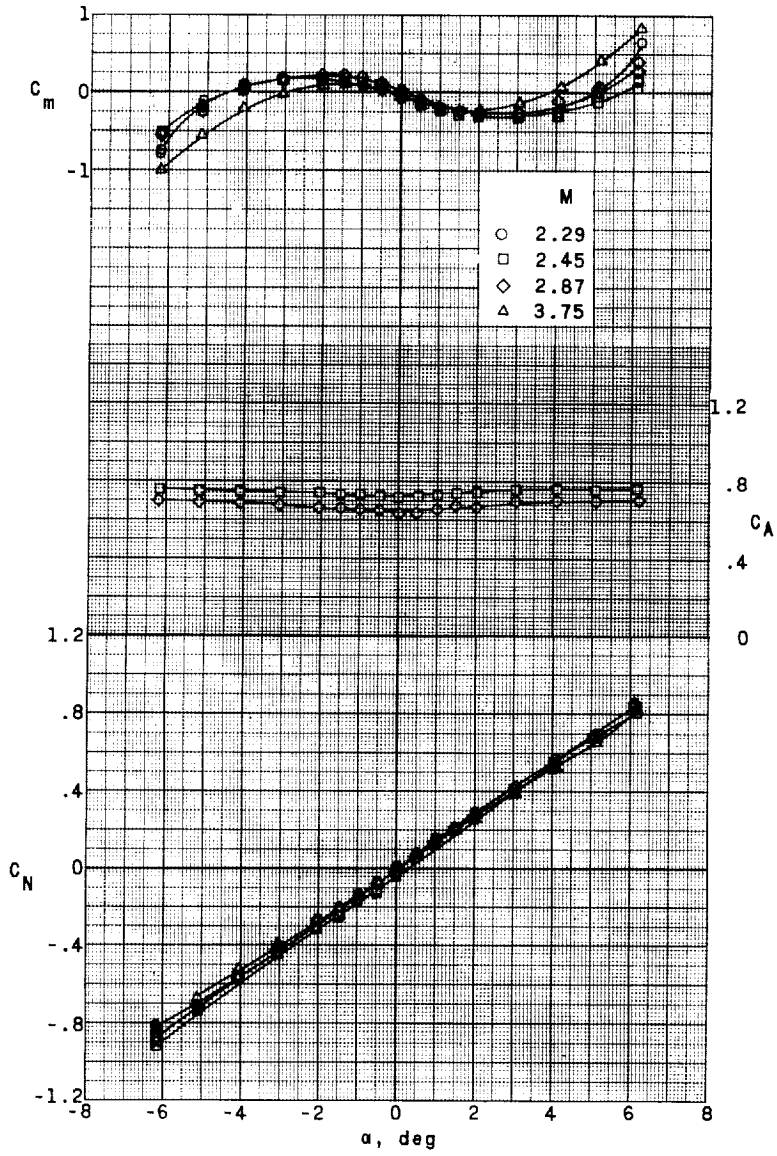


(f) Model $B_1S_1F_1T_1A_1$.

Figure 6.- Concluded.

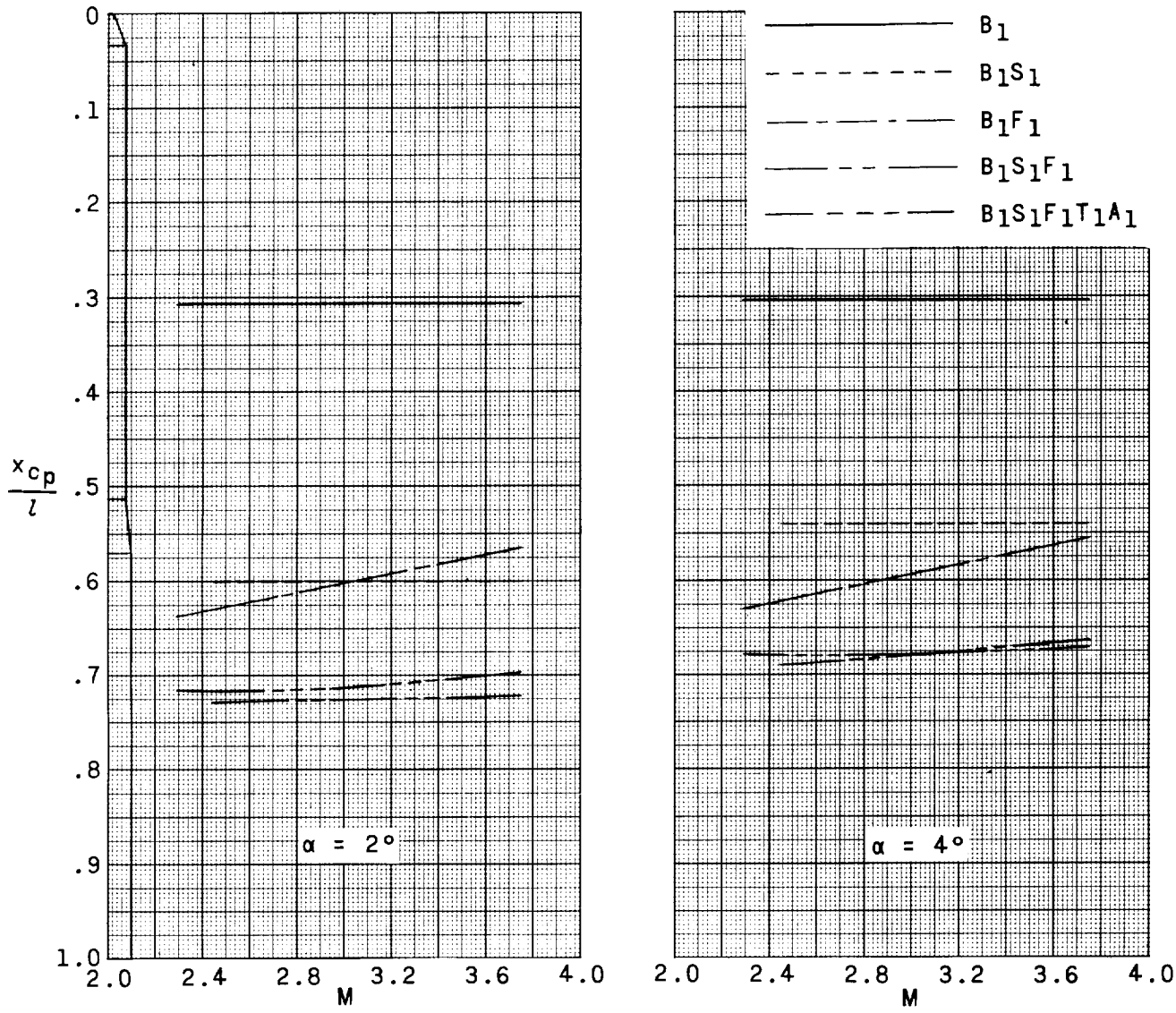


Figure 7.- Center-of-pressure location referenced to body length for Blue Scout model.

The aerodynamic characteristics in sideslip for the Blue Scout model near zero angle of attack (fig. 8(a)) indicates a positive effective dihedral apparently because of the small negative angle of attack. Near $\alpha \approx 5^\circ$ (fig. 8(b)) the effective dihedral becomes highly negative and erratic. A comparison of figures 8(a) and 8(b) shows that the model becomes considerably more unstable in yaw as $\alpha$ is increased from about $0^\circ$ to $5^\circ$. A comparison of figures 8(a) and 8(c) shows that the addition of antennas has a negligible effect on the lateral characteristics near $\alpha = 0^\circ$. A comparison of figures 8(b) and 8(d) indicates that for $\alpha \approx 5^\circ$ the addition of antennas produces generally higher values of $C_l$. The antennas appear to have only a small effect on $C_n$ and $C_Y$. As in the case of model $B_1S_1F_1T_1$, model $B_1S_1F_1T_1A_1$ shows a decrease in directional stability as $\alpha$ is increased from $0^\circ$ to $5^\circ$.

## Blue Scout, Jr., Configuration

The aerodynamic characteristics in pitch for the various components of Blue Scout, Jr., model are shown in figure 9. All configurations exhibit a relatively linear variation of $C_m$ and $C_N$ with angle of attack. Some interference effects apparently exist between the forward and the rearward fins inasmuch as the $C_N$ and $C_m$ values for the model with both sets of fins on are less than would be expected from a summation of their separate effects. The center-of-pressure location as a fraction of body length for angles of attack of $2^\circ$ and $4^\circ$ are presented in figure 10. For the angles of attack presented, all finned configurations show a forward movement of the center of pressure with increasing Mach number, reflecting the loss in fin effectiveness.

The aerodynamic characteristics in sideslip for the Blue Scout, Jr., model are presented in figure 11. The rolling moment due to sideslip is similar to that for the Blue Scout model (fig. 8) with a slightly positive dihedral effect indicated near zero angle of attack (fig. 11(a)) and a negative dihedral effect indicated at $\alpha = 4.9^\circ$ (fig. 11(b)). However, the effect of $\alpha$ on $C_n$ and $C_Y$ appears to be relatively small.

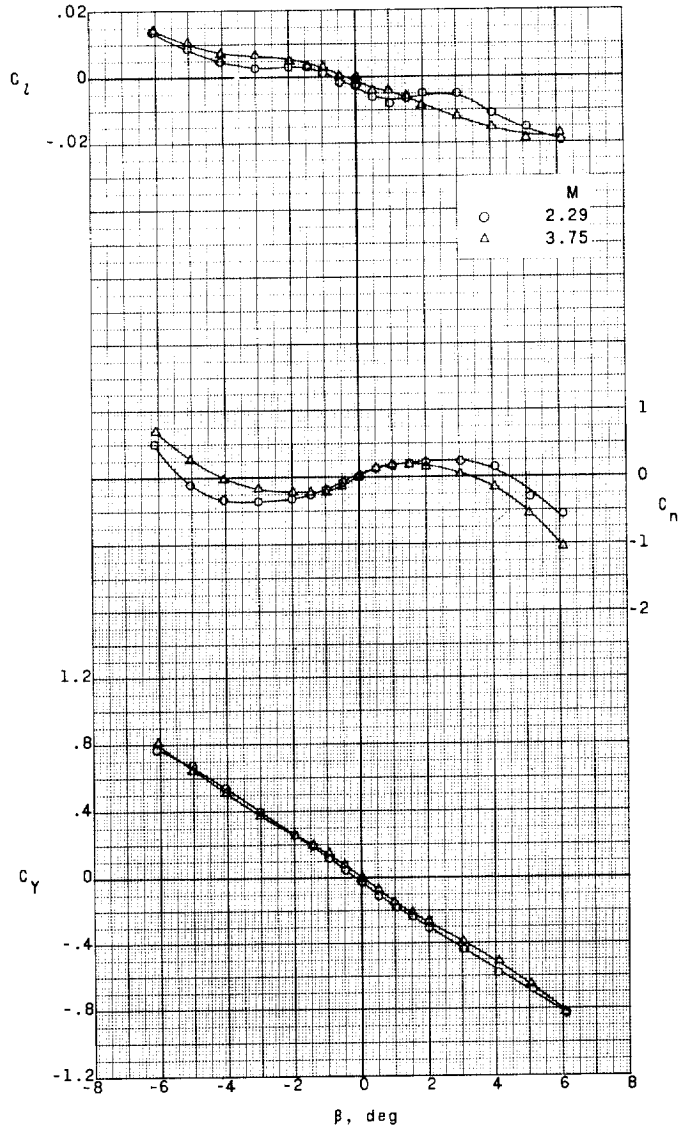


(a) Model $B_1S_1F_1T_1$; $\alpha = -0.2^{\circ}$.

Figure 8.- Aerodynamic characteristics in sideslip of a 0.067-scale model of Blue Scout configuration.

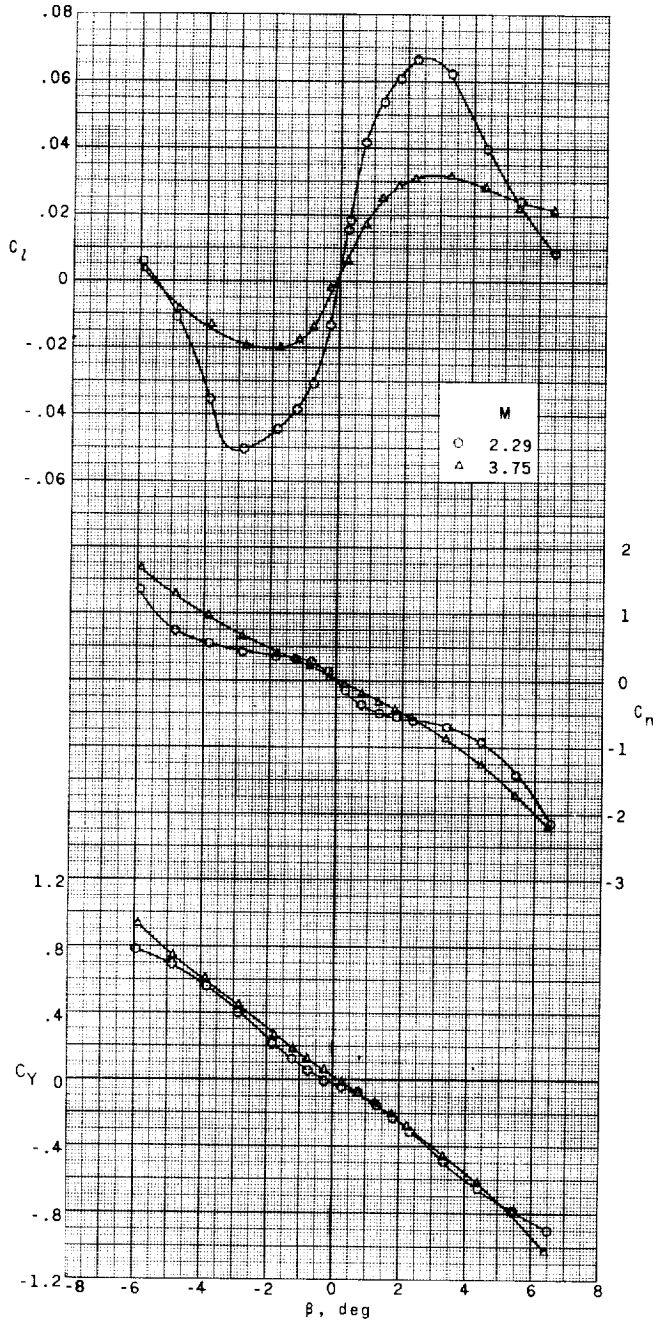


(b) Model $B_1S_1F_1T_1$; $\alpha = 4.9^{\circ}$.

Figure 8.- Continued.

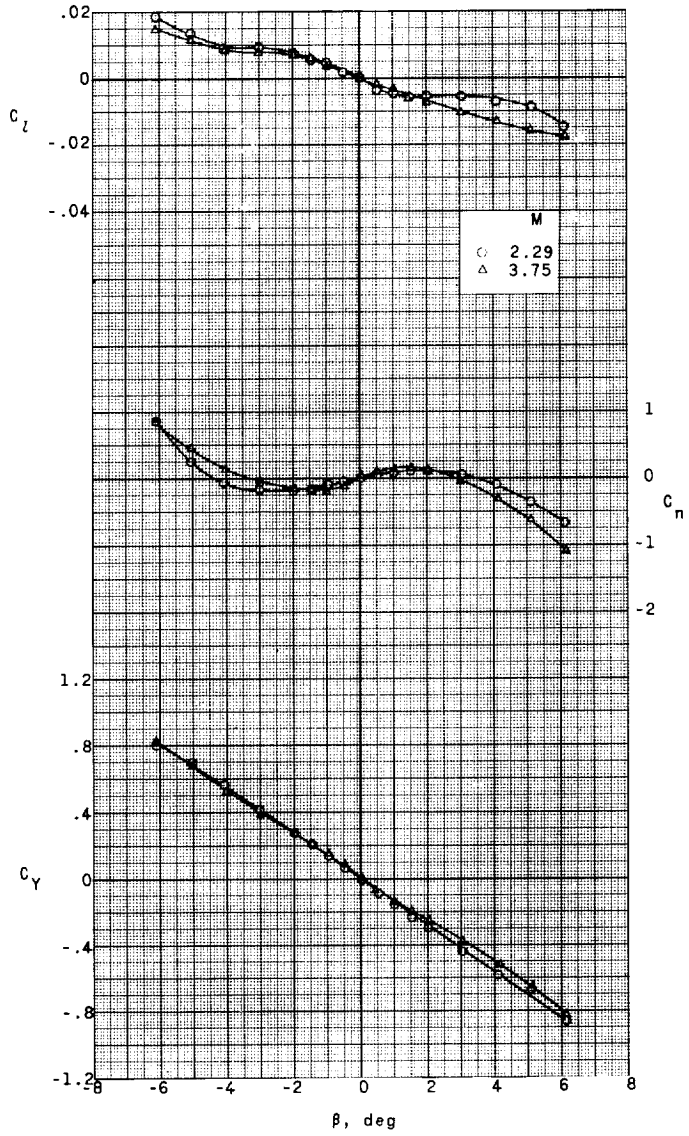


(c) Model $B_1S_1F_1T_1A_1$; $\alpha = -0.1^{\circ}$.

Figure 8.- Continued.

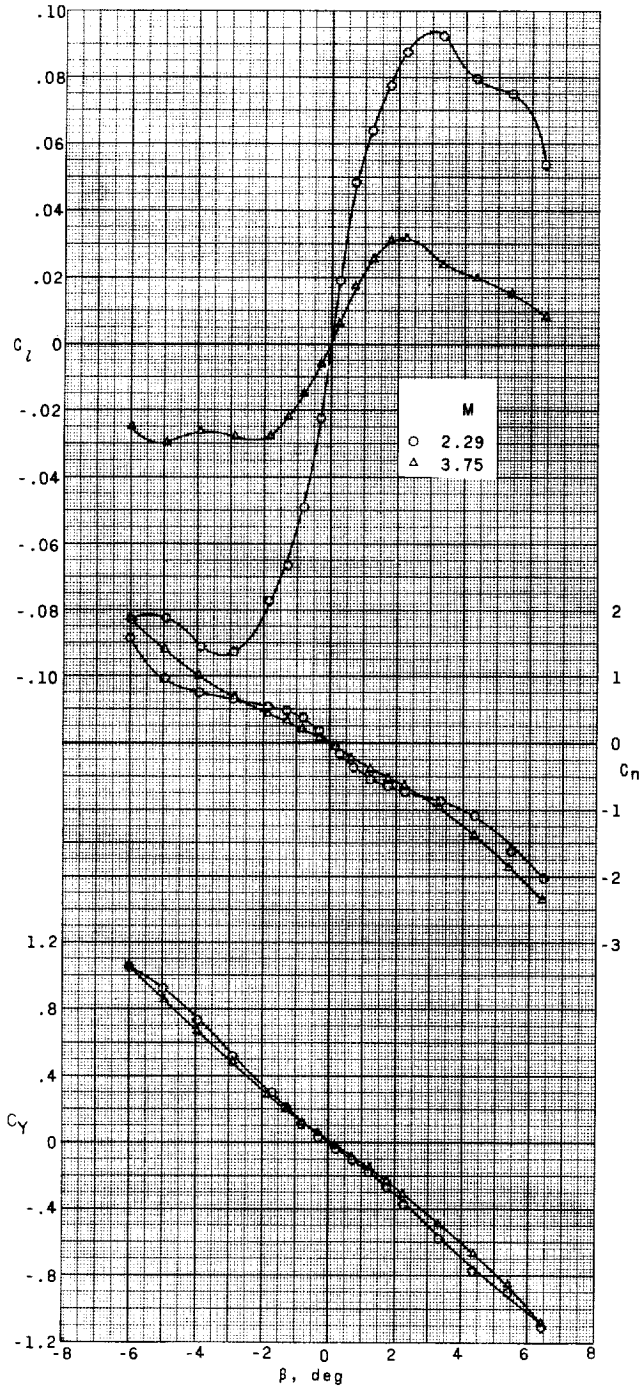


(d) Model $B_1S_1F_1T_1A_1$; $\alpha = 5.0°$.

Figure 8.- Concluded.

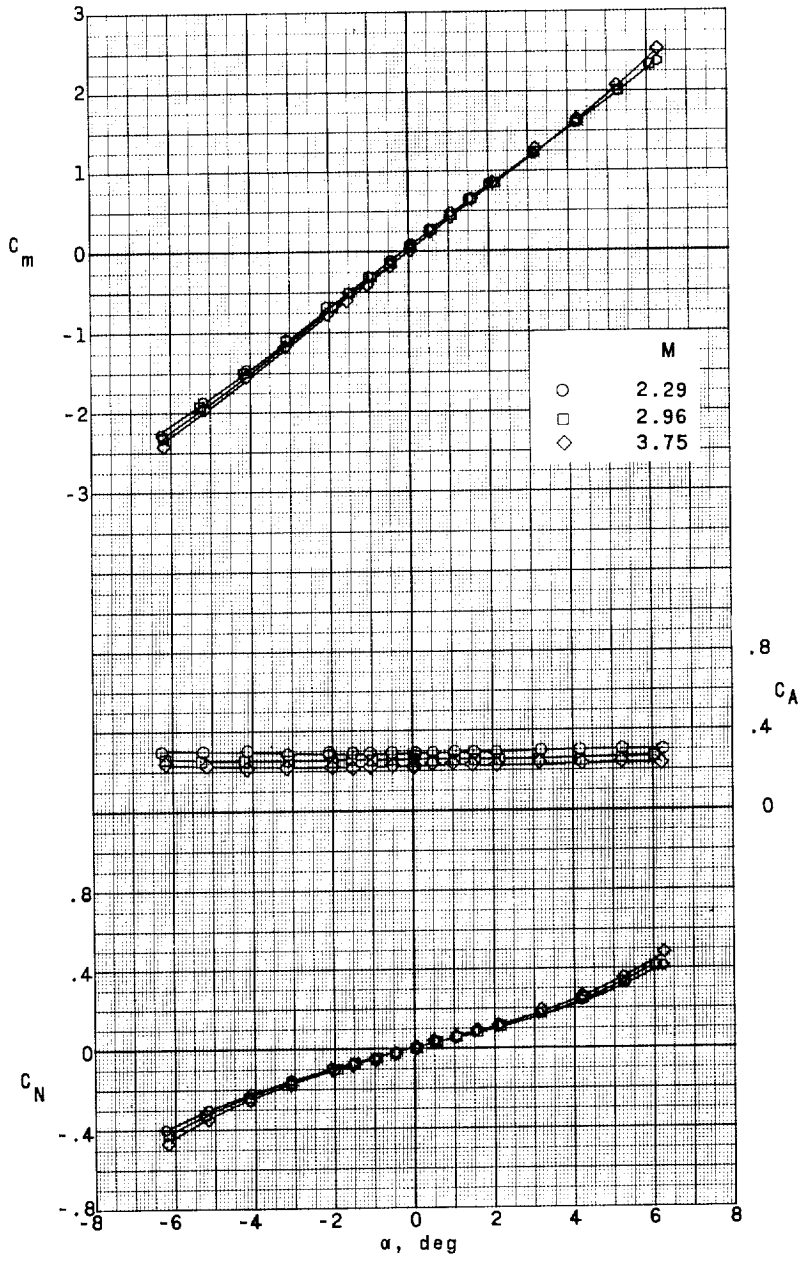


(a) Model $B_2$.

Figure 9.- Aerodynamic characteristics in pitch of a 0.100-scale model of the Blue Scout, Jr., configuration.

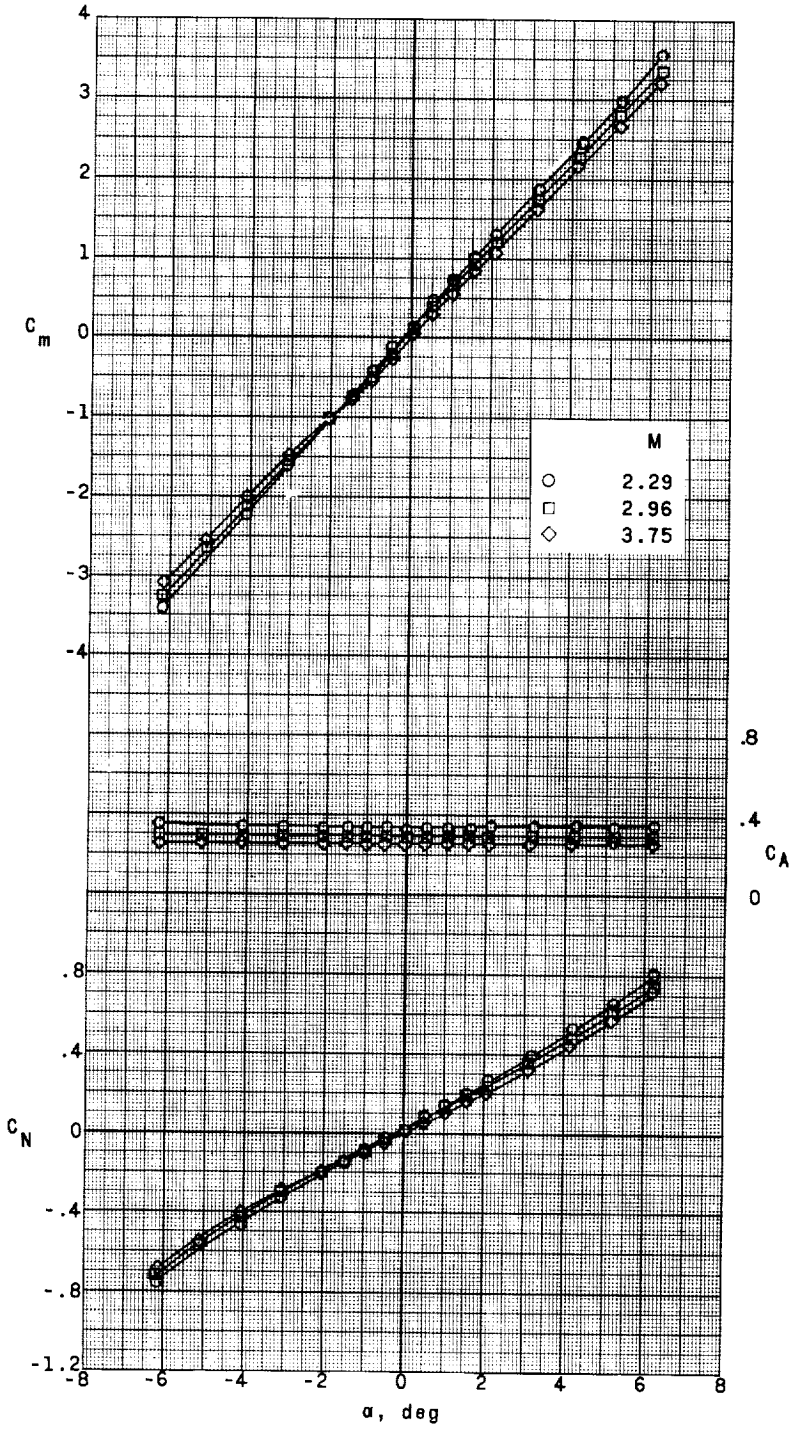


(b) Model $B_2F_{21}$.

Figure 9.- Continued.

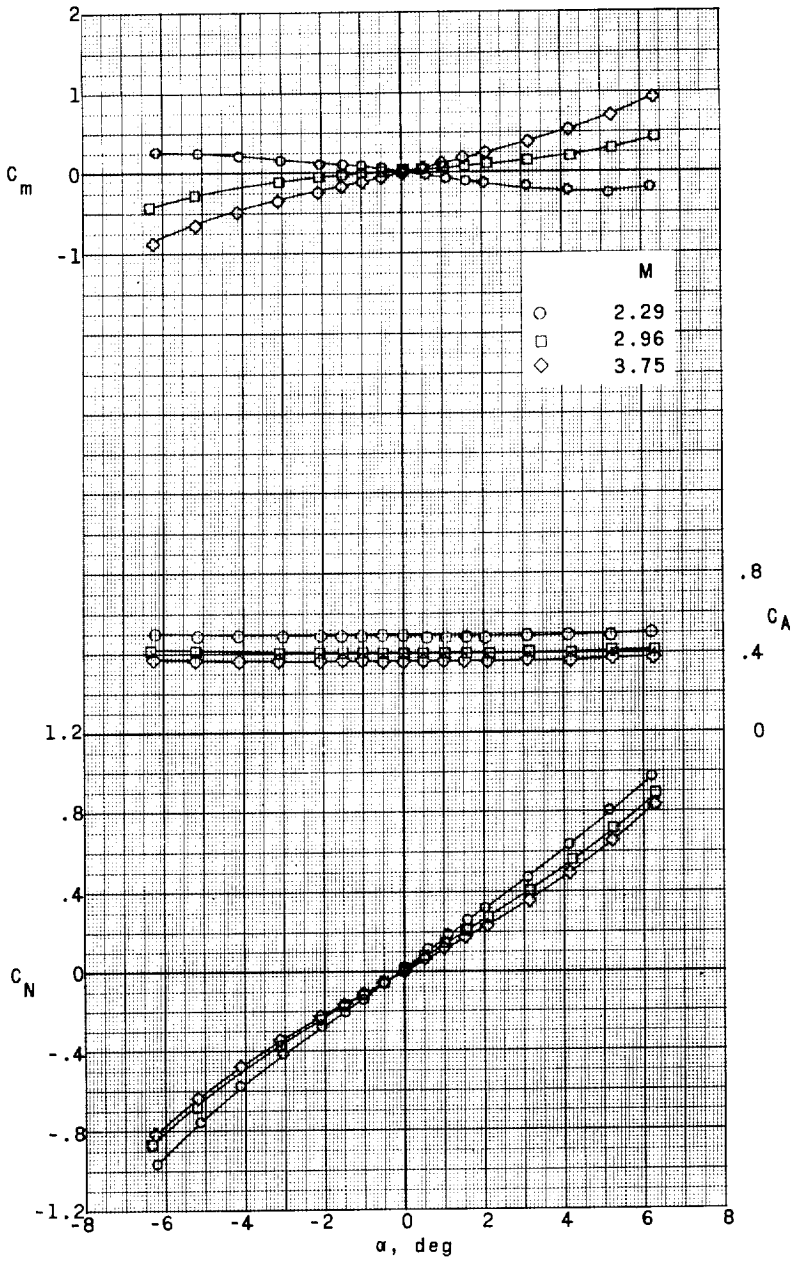


(c) Model $B_2F_{22}$.

Figure 9.- Continued.

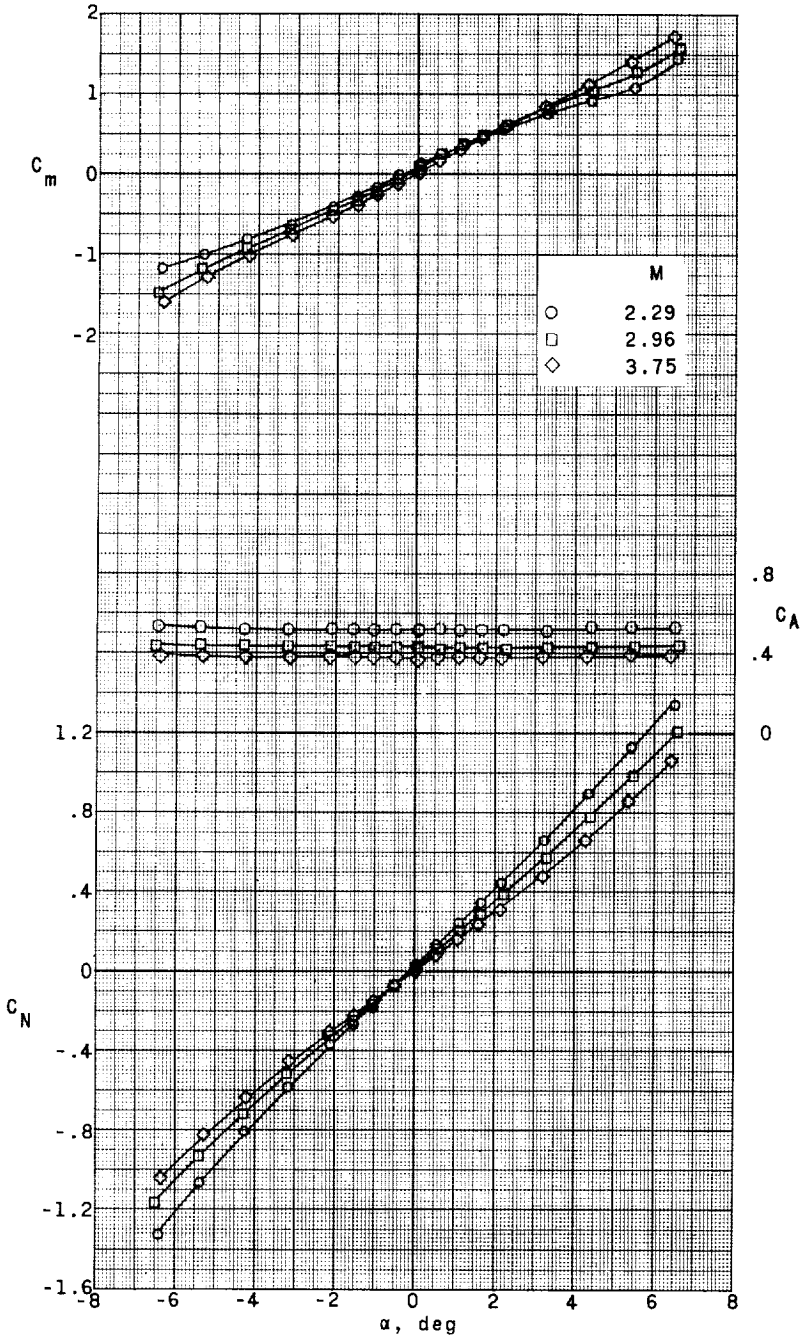


(d) Model $B_2F_{21}F_{22}$.

Figure 9.- Concluded.

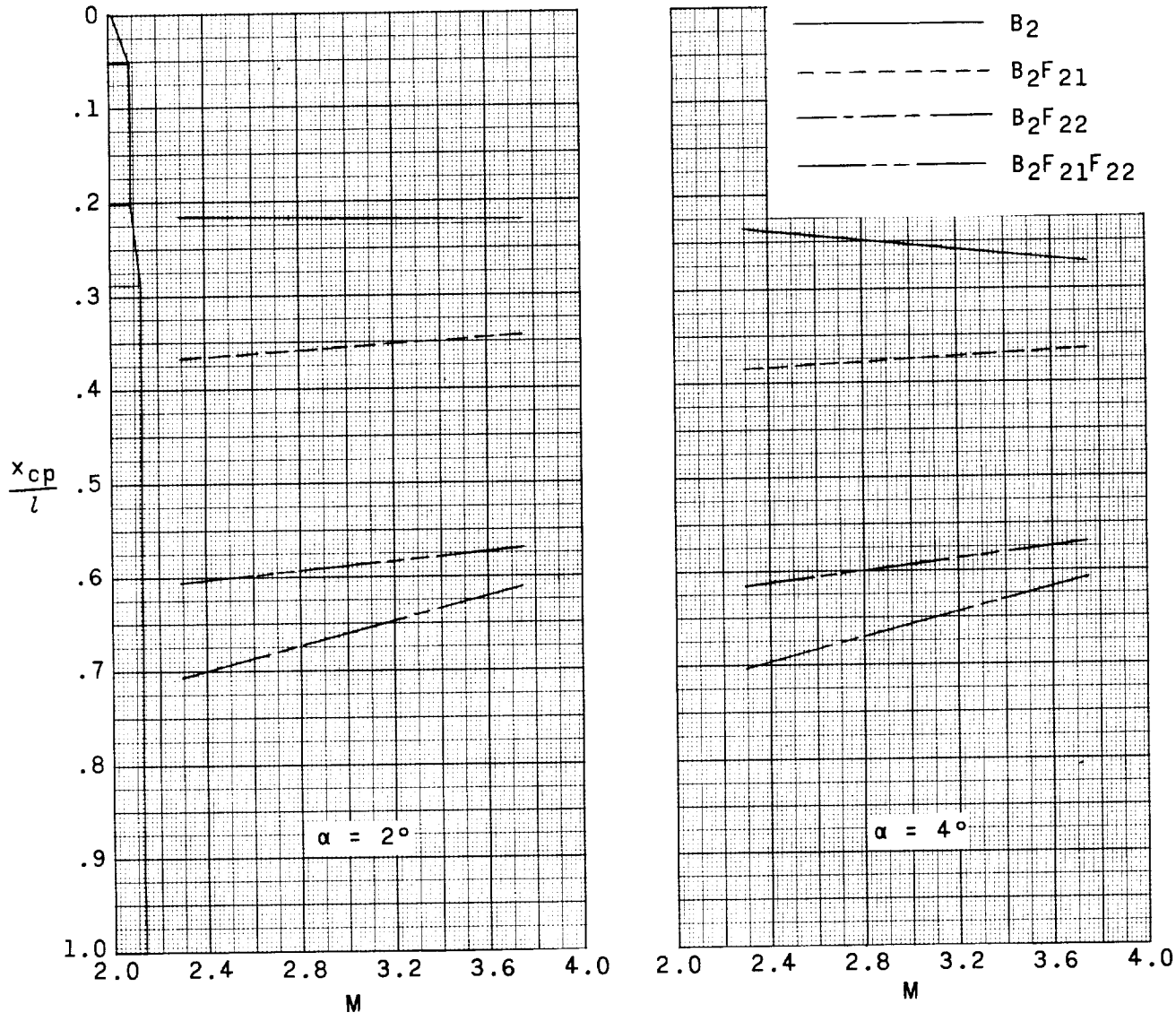


Figure 10.- Center-of-pressure location referenced to body length for Blue Scout, Jr., configuration.

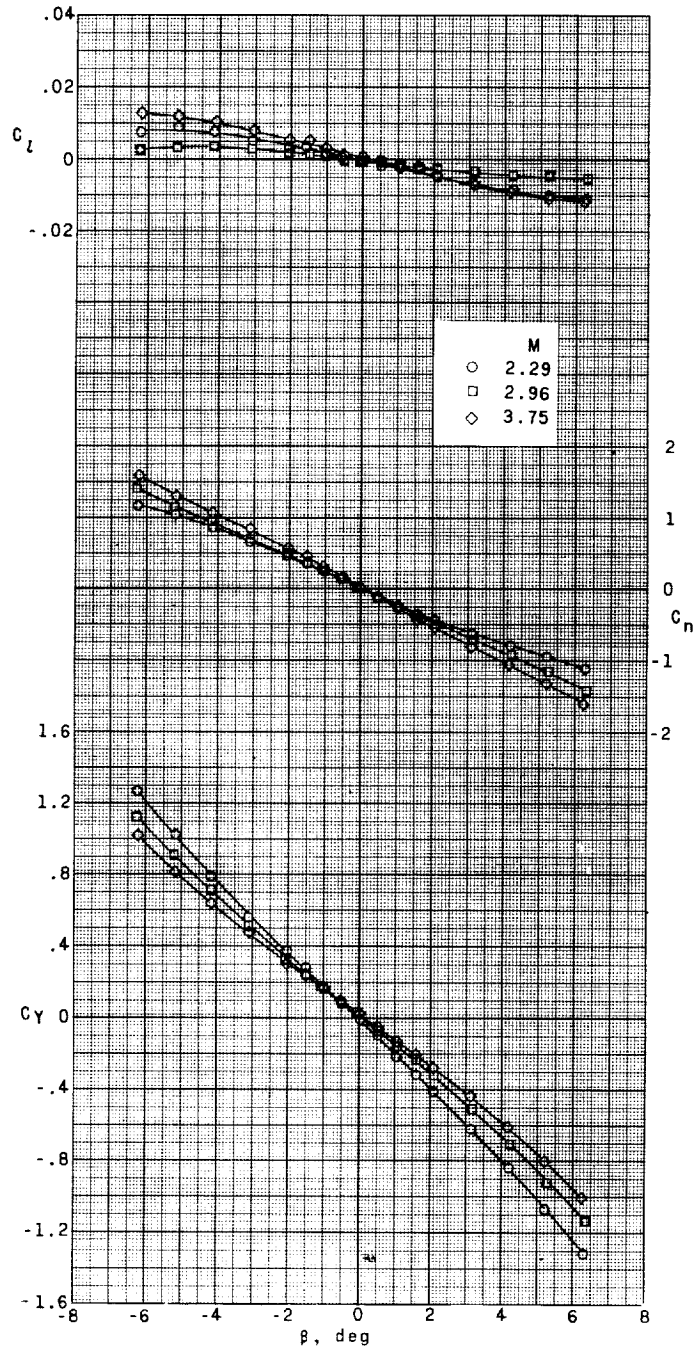


(a) Model $B_2F_{21}F_{22}$; $\alpha = -0.3^{\circ}$.

Figure 11.- Aerodynamic characteristics in sideslip of a 0.100-scale model of Blue Scout, Jr., configuration.

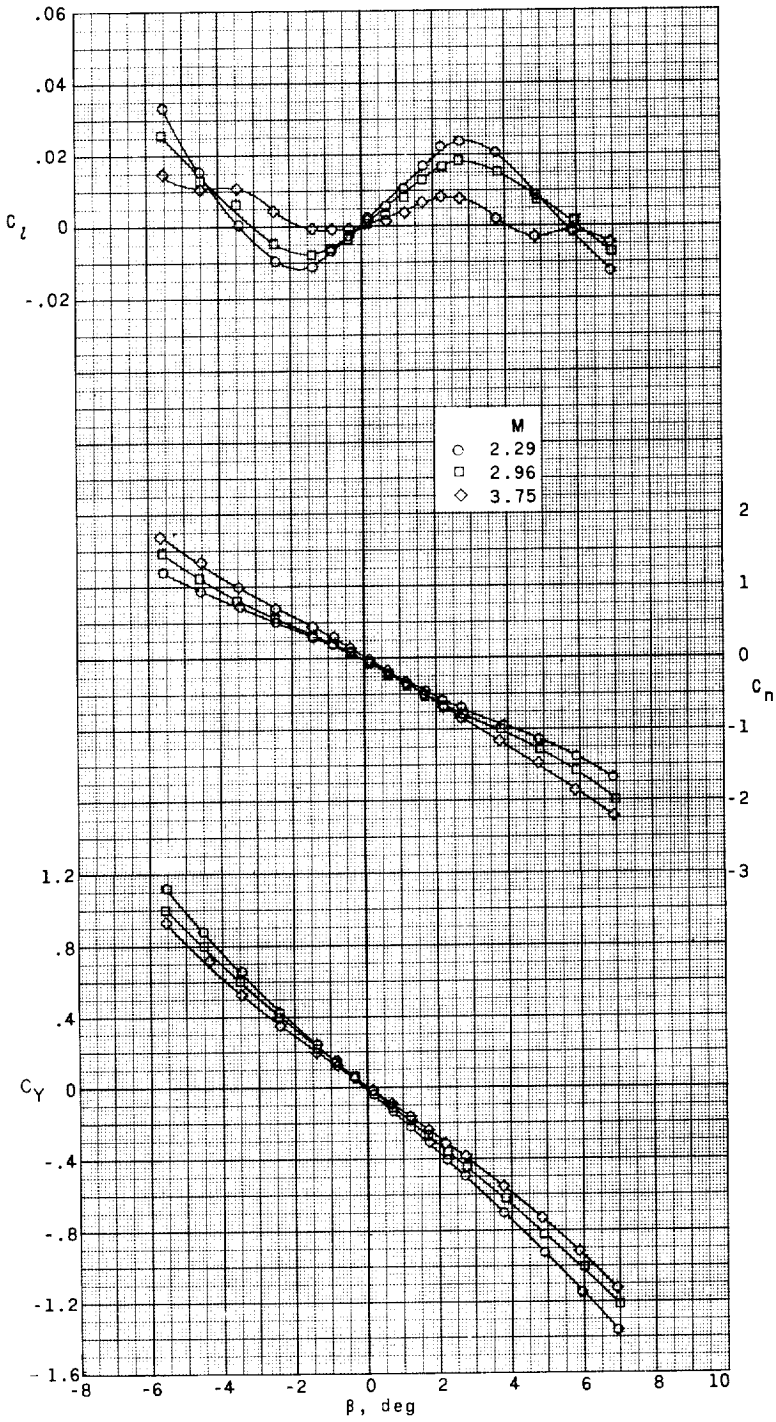


(b) Model $B_2F_{21}F_{22}$; $\alpha = 4.9^{\circ}$.

Figure 11.- Concluded.

## CONCLUSIONS

An investigation has been conducted to determine the static longitudinal and lateral stability characteristics of the Blue Scout and the Blue Scout, Jr., and the effects of their various components through the Mach number range from 2.29 to 3.75. The results indicate the following conclusions:

1. The complete models of both the Blue Scout and the Blue Scout, Jr., exhibit a slight forward shift in the center-of-pressure location with increasing Mach number.

2. Both models indicated a relatively small positive effective dihedral near $\alpha = 0^\circ$; however, at $\alpha = 5^\circ$ the effective dihedral becomes highly negative, especially at the lower test Mach number.

3. A small amount of flare-fin interference effect was exhibited by the Blue Scout configuration. There was an interference between the forward and rearward fins of the Blue Scout, Jr., configuration.

Langley Research Center,
National Aeronautics and Space Administration,
Langley Station, Hampton, Va., May 6, 1963.

## REFERENCES

1. Kelly, Thomas C.: Transonic Wind-Tunnel Investigation of the Static Longitudinal Aerodynamic Characteristics of Several Configurations of the Scout Vehicle and of a Number of Related Models. NASA TN D-794, 1961.

2. Robinson, Ross B.: Aerodynamic Characteristics in Pitch and Sideslip of a 1/15-Scale Model of the Scout Vehicle at a Mach Number of 2.01. NASA TN D-793, 1961.

3. Jernell, Lloyd S., and Wong, Norman: Investigation of the Static Longitudinal Stability Characteristics of a 0.067-Scale Model of a Four-Stage Configuration of the Scout Research Vehicle at Mach Numbers of 2.29, 2.96, 3.96, and 4.65. NASA TN D-554, 1960.

4. Jernell, Lloyd S.: Investigation of the Static Longitudinal and Lateral Stability Characteristics of a 0.10-Scale Model of a Three-Stage Configuration of the Scout Research Vehicle at Mach Numbers of 2.29, 2.96, 3.96, and 4.65. NASA TN D-711, 1961.